

View Article Online

# **EES Batteries**

# Accepted Manuscript

This article can be cited before page numbers have been issued, to do this please use: S. Xia, L. Yan, N. Wang, Q. Zhou, L. Liu, B. Peng, T. Wang, F. Wang, J. He, Y. Ma and Y. Wu, *EES Batteries*, 2025, DOI: 10.1039/D5EB00160A.



This is an Accepted Manuscript, which has been through the Royal Society of Chemistry peer review process and has been accepted for publication.

Accepted Manuscripts are published online shortly after acceptance, before technical editing, formatting and proof reading. Using this free service, authors can make their results available to the community, in citable form, before we publish the edited article. We will replace this Accepted Manuscript with the edited and formatted Advance Article as soon as it is available.

You can find more information about Accepted Manuscripts in the <u>Information for Authors</u>.

Please note that technical editing may introduce minor changes to the text and/or graphics, which may alter content. The journal's standard <u>Terms & Conditions</u> and the <u>Ethical guidelines</u> still apply. In no event shall the Royal Society of Chemistry be held responsible for any errors or omissions in this Accepted Manuscript or any consequences arising from the use of any information it contains.



View Article Online DOI: 10.1039/D5EB00160A

**Batteries Accepted Manuscript** 

### **ARTICLE**

# Li<sub>0.95</sub>Na<sub>0.05</sub>FePO<sub>4</sub> as a trifunctional additive to boost the electrochemical performance of cathodes in lithium-sulfur batteries

Received 00th January 20xx, Accepted 00th January 20xx

DOI: 10.1039/x0xx00000x

Shuang Xia,<sup>a†</sup> Luo Yan,<sup>b†</sup> Nan Wang,<sup>a</sup> Qi Zhou,<sup>a</sup> Lili Liu,<sup>\*c</sup> Bohao Peng,<sup>a</sup> Tao Wang,<sup>\*a</sup> Faxing Wang,<sup>a</sup> Jiarui He<sup>a</sup>, Yuan Ma<sup>a</sup>, and Yuping Wu<sup>a\*</sup>

#### **Broader context**

Lithium-sulfur batteries (LSBs) are regarded as leading candidates for next-generation energy-efficient vehicles due to their high theoretical energy density. However, conventional sulfur cathodes suffer from insufficient adsorption of polysulfide intermediates and poor catalytic conversion, leading to low utilization efficiency of active sulfur substances. Moreover, the thickness of sulfur cathodes can reach tens of micrometers, and the insulating nature of elemental sulfur hinders the effective movements of electrons and Li<sup>+</sup> ions. We initially propose micron-sized Li<sub>0.95</sub>Na<sub>0.05</sub>FePO<sub>4</sub> (LNFP), a Na<sup>+</sup>-doped LFP derivative with enhanced ionic conductivity, as a cathode additive to address these challenges. Our studies reveal that Na<sup>+</sup> doping effectively exposes more adsorption sites in LFP and enhances polysulfide adsorption via polythionate complex formation, with complete desorption achievable during redox cycling. Simultaneously, Na<sup>+</sup> doping alters the electronic environment of Fe<sup>2+</sup>/Fe<sup>3+</sup>, thereby boosting the inherent electronic conductivity of the LFP. Consequently, this enables the LNFP to convert adsorbed polysulfides into sulfides and S<sup>2-</sup> more effectively. Additionally, Na<sup>+</sup> doping widens ion migration channels for Li<sup>+</sup>, which leads to an increased ionic conductivity. Benefiting from the aforementioned triple functions of the LNFP, the assembled LSBs exhibit excellent cycling stability at 1 C, along with outstanding kinetic performance even under high sulfur loading and at high current density. This work provides novel insights into the design and fabrication of high-performance cathode additives, offering concrete guidance to facilitate the commercialization of advanced LSBs.

Lithium-sulfur batteries (LSBs) are regarded as one of the effective candidates for next-generation energy storage systems due to their high energy density. Conventional sulfur cathodes suffer from inadequate polysulfide adsorption and catalytic conversion capabilities, along with sluggish ion kinetics, leading to low utilization of active sulfur substances. These limitations hinder the practical application of LSBs. Here, a micrometer-sized LNFP (Li<sub>0.95</sub>Na<sub>0.05</sub>FePO<sub>4</sub>) with enhanced ion conductivity is innovatively proposed as an additive for the cathode to address this challenge. Through theoretical analysis (density functional theory, DFT) and

empirical experiments, it is found that Na<sup>+</sup> doping not only exposes effective adsorption sites but also alters the electronic environment of Fe<sup>2+</sup> /Fe<sup>3+</sup>, thereby enhancing the adsorption and catalytic conversion abilities of the LFP towards polysulfides. Multifunctional LNFP additive contributes to high-performance for S cathodes. As a result, the assembled LSB with the LNFP additive delivers an initial discharge specific capacity of 953 mAh g<sup>-1</sup> at 1 C, exhibits excellent cycling performance with a capacity decay of only 0.039% per cycle after 700 cycles. The prepared LSB retains a specific discharge capacity of 548 mAh g<sup>-1</sup> after 300 cycles at 5 C. The LSB demonstrates a discharge specific capacity of 880 mAh g<sup>-1</sup> under a high sulfur loading of 4.5 mg cm<sup>-2</sup>. This work opens up new avenues for optimizing the performance of LSBs.

#### Introduction

The vigorous development of the market is driving researchers to delve deep into the exploration of cutting-edge energy storage devices. [1-5] Among them, the research and development of secondary

<sup>&</sup>lt;sup>a</sup> Confucius Energy Storage Lab, School of Energy and Environment & Z Energy Storage Center, South East University, Nanjing, Jiangsu, 211189, China

b. School of Mathematics and Physics, University of South China, Hengyang, Hunan, 421001 China

<sup>&</sup>lt;sup>c</sup> State Key Laboratory of Materials-oriented Chemical Engineering & School of Energy Science and Engineering, Nanjing Tech University, Nanjing 211816, China

<sup>†</sup>S. X. and L. Y. contributed equally to this work.

ES Batteries Accepted Manuscript

batteries with high capacity and long lifespan has become an unstoppable trend. With its exceptional high energy density (2600 Wh kg<sup>-1</sup>) and outstanding specific capacity (1675 mAh g<sup>-1</sup>), the lithiumsulfur battery (LSB) precisely aligns with the urgent demands of current market development. [6-9] However, the active sulfur substances on the cathode side react with lithium ions (Li<sup>+</sup>) to form soluble polysulfides during the operation of LSBs. These formed polysulfides freely shuttle between the cathodes and anodes, triggering the so-called 'shuttle effect', which leads to irreversible loss of active materials. Besides, the inherently limited ionic conductivity of sulfur cathodes makes it difficult for the redox couple of S/S<sup>2</sup>especially for thick S cathodes. The above issues significantly constrain the potential of LSBs in practical applications. [10-16] A wide variety of sulfur host materials, encompassing extensive carbon-based materials<sup>[17-22]</sup> and inorganic compounds<sup>[23-25]</sup> are meticulously designed to curb the irreversible loss of active sulfur substances. Regrettably, carbon-based materials inherently possess limited anchoring abilities for active substances. Modifying carbon materials, such as grafting active functional groups onto their surfaces, can effectively enhance the anchoring ability of carbon materials toward polysulfides. However, this will inevitably increase the manufacturing cost of the cathode. Due to the inherently poor conductivity and the weak electrochemical activity of the sulfur, relying solely on the tailored sulfur host does not enhance the kinetic performance of redox reactions in LSBs. Furthermore, even if inorganic compounds with special functionalities are prepared for use as sulfur hosts, they still face the issue of escalating production costs. Therefore, constructing a high-performance cathode to enhance the overall performance of LSBs is currently a major technical challenge. Among the various cathode modification strategies, the introduction of functional additives to promote reaction kinetics is recognized as a highly promising and feasible approach.[26-28]

Outstanding ionic conductivity stands as a pivotal characteristic indicator among functional additives, ensuring efficient ion transport. Recent research revealed that lithium salts with certain ionic conductivities such as LTO (Li<sub>4</sub>Ti<sub>5</sub>O<sub>12</sub>)<sup>[29]</sup> and LFP (LiFePO<sub>4</sub>),<sup>[30]</sup> which combine high stability with environmental friendliness, exhibit potential as modified materials for separators in LSBs. Research reports on the use of such lithium salts as functional additives for cathodes are extremely scarce. To the best of our knowledge, there is still a gap in the research on successfully preparing additives with higher ionic conductivity based on these materials in LSBs. Modifying these materials can further enhance their ionic conductivities. Delving deeper into this field will undoubtedly greatly broaden the selection of additives and open up new avenues for the development of high-performance cathodes. In particular, the adsorption capacity of the LFP for polysulfides further confirms its feasibility and application value as an additive for the cathode. [31] The LFP can also facilitate the migration of Li+ cations in LSBs. Furthermore, modifying the LFP can further enhance its performance, thereby strengthening its applicability in LSBs. Research findings indicate that incorporating dopant atoms (Zr, Mg, Co, or Na)[32] into the LFP is proven to be an effective means of enhancing its ionic conductivity. The performance of doped LFP-based materials in LSBs remains to be thoroughly explored. In addition, micrometer-sized additives reduce the requirements for production equipment compared to nanomaterials in production and practical application by provides favorable conditions for their large-scale productions for their large-scale productions.

In previous research, we successfully synthesized a micrometersized Li<sub>0.95</sub>Na<sub>0.05</sub>FePO<sub>4</sub> (LNFP) and revealed that compared to the LFP, the LNFP exhibits higher ionic conductivity. [33] Building on this foundation, this work initially validated the practical feasibility of using the LNFP as a cathode additive in the LSB. The enhanced ionic conductivity enables effective inward diffusion of polysulfides toward the cathode interior. Specifically, we find that the Na<sup>+</sup> doping widens the ion channels of the LFP, which implies that the LNFP can offer more sites for the adsorption of polysulfides. Meanwhile, Na<sup>+</sup> doping improves the intrinsic electronic conductivity of the LFP, thereby enhancing its catalytic conversion ability towards polysulfides. The LNFP improves the utilization of active sulfur substances through trifunctionality in ion migration, adsorption, and catalysis. As expected, the LSB employing the LNFP as a cathode additive exhibits excellent electrochemical performance. This innovative research provides a valuable reference for the large-scale production of additives. The work carries immense and groundbreaking significance for advancing the commercialization process of high-performance cathodes.

#### Results and discussion

The LNFP particles were prepared via a sintering method and subsequently underwent comprehensive characterization. The XRD patterns (Fig. S1) reveal that the diffraction peaks of the prepared LNFP particles are consistent with those of the LFP (JCPDS No. 81-1173). This result indicates that the doping of trace amounts of Na atoms does not cause any alteration to the original olivine-type structure of the LFP. Through EDS (energy dispersive spectrometer) testing (Fig. S2), sodium elements are found to be uniformly distributed in the LNFP. The XPS (X-ray photoelectron spectroscopy) test results also reveal the presence of peaks corresponding to Na (Fig. S3).[34] These results are consistent with our previous findings,[33] indicating the successful preparation of the LNFP. Through observation via scanning electron microscope (SEM) images (Fig. S4), it is evident that the LNFP exhibits irregular morphological features with dimensions in the micrometer range, which is conducive to large-scale production. It can be seen from the nitrogen adsorptiondesorption isotherm that the isotherm of the LNFP (Fig. S5a) is similar to the LFP. The Brunauer-emmer-teller (BET) surface area of the LNFP is 11 m<sup>2</sup> g<sup>-1</sup>, which is higher than that of the LFP (9 m<sup>2</sup> g<sup>-1</sup>). This difference serves as Na doping widens the ion diffusion channels. The pore size distribution of the LNFP is primarily concentrated around approximately 5 nm (Fig. S5b).

The LNFP/Li (the cathode was the LNFP electrode, the anode was the lithium foil, and the electrolyte was LS-009) cell was assembled to validate the feasibility of using the LNFP as an additive for the cathode in the LSB. A cyclic voltammetry (CV) test is conducted on the cell at a scan rate of 0.1 mV s<sup>-1</sup>, and the results show no responsive current is generated (Fig. S6a). This indicates that the LNFP does not participate in redox reactions independently during the operation of the LSB. Similarly, charge-discharge tests are performed on the cell at 0.13 mA, and no capacity contribution is observed (Fig. S6b). Furthermore, inside an argon-filled glove box, the LNFP/Li cells with Li<sub>2</sub>S<sub>6</sub> electrolytes (after 50 and 100 cycles) were

This article is licensed under a Creative Commons Attribution-NonCommercial 3.0 Unported Licence.

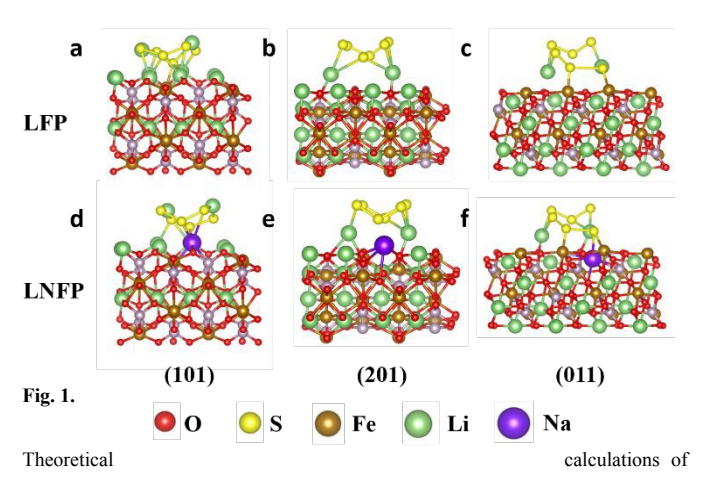
Open Access Article. Published on 08 Oktober 2025. Downloaded on 16.10.25 03:04:51

**ARTICLE Journal Name** 

disassembled. Subsequently, the LNFP electrodes were cleaned and dried. Afterward, these electrodes underwent XRD testing and were compared with an unreacted LNFP electrode. The results reveal an excellent degree of consistency among the XRD diffraction peaks of these three electrodes (Fig. S7). This finding strongly supports the feasibility of the LNFP as a cathode additive.

Aluminum foils coated with the LNFP were cut into small circular pieces and assembled as electrodes to form symmetric cells with Li<sub>2</sub>S<sub>6</sub> electrolytes, aiming to evaluate the catalytic ability of the LNFP towards polysulfides. Additionally, a symmetric cell using pure electrolyte (LS-009) was assembled as a control for comparative analysis. Through the analysis of CV curves (Fig. S8), it is observed that under a scan rate of 5 mV s<sup>-1</sup>, the LNFP symmetric cell with pure electrolyte does not exhibit any noticeable response current. Conversely, the symmetric cell with Li<sub>2</sub>S<sub>6</sub> electrolyte demonstrates a significant response current, indicating that the response current originated from the redox reaction of Li<sub>2</sub>S<sub>6</sub>. Notably, compared to the almost negligible response current of the LFP symmetric cell with Li<sub>2</sub>S<sub>6</sub> electrolyte, the LNFP symmetric cell produces a much stronger response current. This finding suggests that Na+ doping can enhance the catalytic conversion efficiency of the LFP towards polysulfides. The reason for this remarkable difference may lie in that the Na<sup>+</sup> doping not only widens the ion diffusion channels in the LFP [33] but also alters the electronic environment of Fe<sup>2+</sup>/Fe<sup>3+</sup>, thereby improving the intrinsic electronic conductivity of the LFP. From the Fe 2p XPS testing results of the LFP and LNFP (Fig. S9), it can be observed that the significant shifts in the peaks corresponding to Fe<sup>2+</sup> and Fe<sup>3+</sup> after Na<sup>+</sup> doping, which demonstrates that the introduction of Na alters the electronic environment of Fe2+/Fe3+. It can be observed that the Li2S nucleation peak current for the C-LNFP electrode appears 14 seconds earlier than that of the C electrode. After the addition of the LNFP, the deposition capacity also increases from the original 100 mAh g<sup>-1</sup> to 147 mAh g<sup>-1</sup> (Fig. S10). This finding further demonstrates the enhanced electrocatalytic activity of the LNFP.[29]

From an experimental perspective, this study aims to reveal the adsorption capacity of the LNFP for polysulfides. Based on the same mass of the LFP and LNFP, the adsorption capacity of different materials for polysulfides is evaluated by observing the color change of the Li<sub>2</sub>S<sub>6</sub> solution. It is found that the Li<sub>2</sub>S<sub>6</sub> solution containing the LNFP became clear and transparent after 12 h (Fig. S11a), indicating that the LNFP has excellent adsorption capacity for polysulfides. From the UV-visible absorption spectrums of the corresponding



the adsorption energies of the LNFP and LFP for the Li<sub>2</sub>S<sub>6</sub>, key: \( a \) \( F\_{\text{ads}\overline{\ove (b) E<sub>ads</sub>=-2.8 eV, (c) E<sub>ads</sub>=-0.2 eV, (d) E<sub>ads</sub>=-4.0 eV, (e) 2½ 10-4.93 eV, (f) 120162.4 eV.

supernatants (Fig. S11b), it can be seen that the absorbance of the LNFP-Li<sub>2</sub>S<sub>6</sub> dispersion is weaker compared to that of the LFP-Li<sub>2</sub>S<sub>6</sub> dispersion, further proving that the LNFP has a stronger adsorption capacity for polysulfides.<sup>[35]</sup>

To delve deeply into the adsorption mechanism of the LNFP towards polysulfides from a theoretical computation perspective, we employed density functional theory (DFT) calculations to analyze the atomic-level interactions between the LNFP, LFP, and polysulfides (Fig.1). Both the LFP and LNFP models are constructed and optimized respectively. The Li<sub>2</sub>S<sub>6</sub> as a representative polysulfide is chosen to investigate the adsorption principles by calculating its binding energy with the aforementioned geometric models. Herein, the adsorption energy (E<sub>ads</sub>) is defined as the total energy when lithium atoms are adsorbed onto the surface, minus the energy of the surface without lithium atom adsorption, further subtracted by the energy of the isolated lithium ion. After calculations, the adsorption energies of different adsorption surfaces on the LFP for Li<sub>2</sub>S<sub>6</sub> are found to be -2.4 eV, -2.8 eV, and -0.2 eV, respectively. Excitingly, the corresponding adsorption energies on the LNFP reach as high as -4.0 eV, -4.3 eV, and -2.1 eV. This result indicates that the Na<sup>+</sup> doping leads to a substantial enhancement in the adsorption ability of the functionalized additive toward polysulfides.[36-38] Compared to the LFP, the LNFP is capable of establishing stronger chemical interactions with polysulfides. When used as a cathode additive, the LNFP can more effectively provide active sites for anchoring polysulfides, thereby significantly suppressing the 'shuttle effect'. Both experimental results and theoretical calculations fully demonstrate the promising application prospects of the LNFP in LSBs.

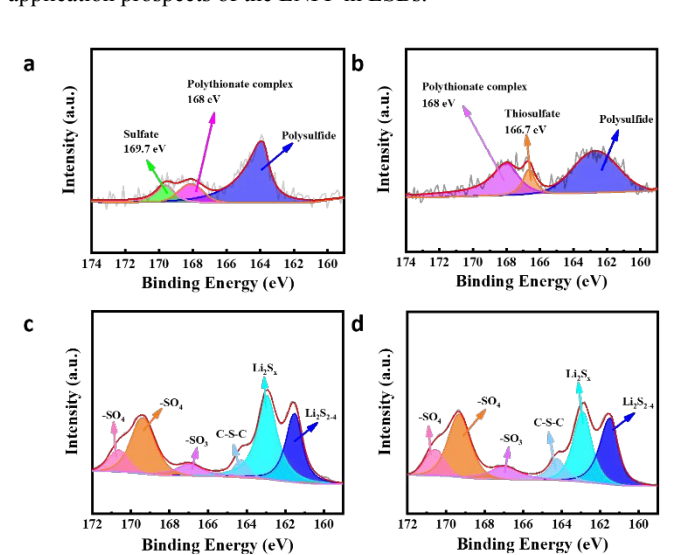


Fig. 2. S 2p XPS spectra of the (a) LFP-Li<sub>2</sub>S<sub>6</sub>, (b) LNFP-Li<sub>2</sub>S<sub>6</sub>, (c) C-S electrode, and (d) C-S-LNFP electrode (discharged to 1.8 V).

The adsorption mechanism of the prepared LNFP towards polysulfides is thoroughly investigated using XPS characterization. After placing equal masses of the LFP and LNFP in Li<sub>2</sub>S<sub>6</sub> solutions and allowing them to stand for 12 hours, the liquid was removed, and the dried solids were subjected to XPS testing. The trace of sulfate at 169.7 eV is generated due to the exposure of the sample to air (Fig.

ARTICLE Journal Name

2a). Peaks corresponding to polythionate complexes can be observed at 168 eV for both samples (Fig. 2b), indicating that polysulfides can combine with the LFP/LNFP to form polythionate complexes, thereby anchoring the polysulfides.<sup>[39]</sup> Besides, the Li<sub>2</sub>S<sub>6</sub>-LNFP sample can also detect a peak belonging to the intermediate product of the thiosulfate at 166.7 eV. By combining theoretical calculations, we infer that LFP-based materials can bind with polysulfides to form polythionate complexes. Additionally, the Na+ doping widens the diffusion channels in the LFP, providing more effective sites for adsorbing polysulfides, resulting in superior polysulfide adsorption of the LNFP compared to the LFP. After discharging the lithium-sulfur cells to 1.8 V, XPS tests were conducted on the C/S electrode and the C/S electrode doped with the LNFP (Figs. 2c and 2d). Two consistent S 2p peaks are observed, indicating that the adsorbed sulfur substance can be completely desorbed from the LNFP during the redox reaction process.

Cathodes doped with the LFP and LNFP were prepared separately, and for comparison, an undoped cathode was also prepared. These cathodes are sequentially labeled as C-S-LFP, C-S-LNFP, and C-S. Subsequently, different cathodes are assembled into lithium-sulfur cells to evaluate the practical effects of various additives in applications. Different assembled cells were subjected to CV testing. The results indicate that the cell with the LNFP additives exhibits CV curves with a large peak area and narrow distance between oxidation

This article is licensed under a Creative Commons Attribution-NonCommercial 3.0 Unported Licence.

Open Access Article. Published on 08 Oktober 2025. Downloaded on 16.10.25 03:04:51

and reduction peaks at 0.1 mV s<sup>-1</sup> (Fig. 3a). This characteristic suggests that the oxidation-reduction reactions in the C-S-LNFP/Li cells proceed fully, with weak polarization phenomena.<sup>[40]</sup> Besides, compared to the C-S/Li and C-S-LFP/Li cells, the C-S-LNFP/Li cells demonstrate excellent overlap in their first three CV curves (Figs. 3b and S12), strongly evidencing that the LNFP can enhance the kinetic process of oxidation-reduction reactions.

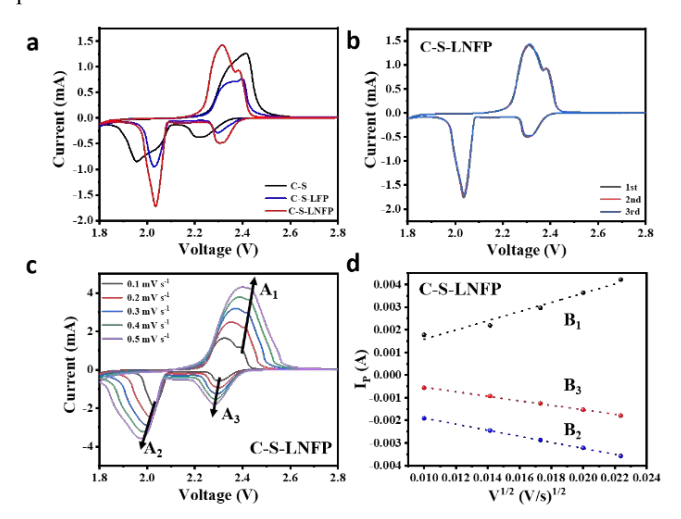


**Fig. 3.** CV tests. (a) First-cycle CV curves of different cells at 0.1 mV s<sup>-1</sup>. (b) CV curves of the C-S-LNFP/Li cell at 0.1 mV s<sup>-1</sup>. (c) CV curves of the C-S-LNFP/Li cell at different scan rates and (d) the corresponding linear matching of peak point currents.

Under various scanning rates, the CV characteristics of different cells were tested. The observation results indicate that even when the scanning rate is increased to 0.5 mV s<sup>-1</sup>, the C-S-LNFP/Li cell still exhibits distinguishable oxidation-reduction peaks (Figs. 3c, S13a, and S13b). By utilizing the linear matching (Figs. 3d, S13c, and

S13d), the Li<sup>+</sup> diffusion coefficients of different batteries le under various voltage conditions were calculated: Upon coefficient of the C-S-LNFP/Li cell is higher than that of the C-S/Li and C-S-LFP/Li cells (Table S1). This advantage is attributed to the enhanced ionic conductivity of the LNFP, which facilitates the rapid migration of Li<sup>+</sup> cations.

After 100 cycles at 1C, different lithium-sulfur cells were subjected to electrochemical impedance spectroscopy (EIS) tests (Fig. S14). Following these cycles, the C-S-LNFP/Li cell exhibits a reduced bulk resistance ( $R_S$ ) in comparison to both the C-S/Li and C-S-LFP/Li cells (Table S2). This indicates that the LNFP as a cathode additive can provide more active reaction sites, which enhances the interaction between the electrolyte and sulfur. Notably, the interfacial resistance  $(R_{SEI})$  of the C-S-LNFP/Li cell is the lowest among the three, suggesting the formation of a more stable SEI (solid electrolyte interface) film during cycling.[41] This phenomenon can likely be attributed to the strong physical adsorption ability of the LNFP for polysulfides, mitigating corrosion of the lithium anode. It is worth noting that the C-S-LNFP/Li cell also displays a low charge transfer resistance  $(R_{CT})$ , an advantage that stems from the inherent excellent ionic conductivity of the LNFP.[42] The low charge transfer resistance of the C-S-LNFP/Li cell also strongly demonstrates that Na doping enhances the intrinsic electronic conductivity of the LFP.

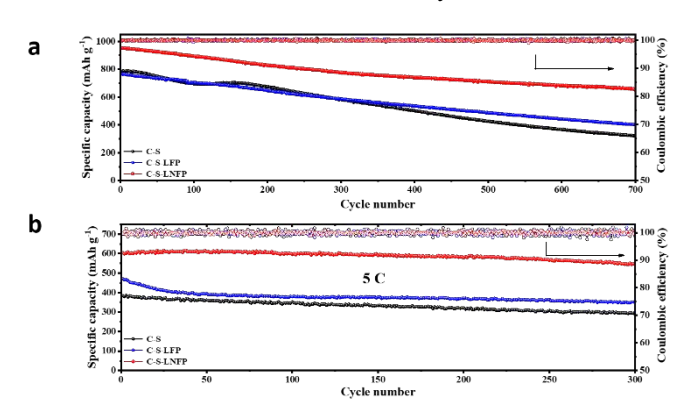


Fig. 4. The cycling performances of different cells at (a)1 C and (b) 5 C.

At 1 C, the initial discharge specific capacities of C-S/Li, C-S-LFP/Li, and C-S-LNFP/Li cells are measured to be 785 mAh g<sup>-1</sup>, 766 mAh g<sup>-1</sup>, and 953 mAh g<sup>-1</sup>, respectively (Fig. 4a). Among them, the C-S-LNFP cell exhibits a superior initial discharge specific capacity, surpassing the other two cells. This performance strongly demonstrates its efficient utilization of active sulfur substances. After 700 cycles, the capacity decay rates per cycle for these three cells are controlled at 0.084%, 0.059%, and a lower 0.039%, respectively. It is gratifying that the discharge specific capacity of the C-S-LNFP/Li cell still attains 652 mAh g-1 after prolonged cycling. The exceptional cycling performance of the C-S-LNFP/Li cell underscores the multiple roles of the LNFP as a cathode additive: it not only suppresses the 'shuttle effect' but also enhances the kinetics of redox reactions. By analyzing the corresponding charge/discharge curves (Fig. S15), it can be observed that the discharge specific capacities of the C-S/Li and C-S-LFP/Li cells exhibit a relatively rapid decay trend. In contrast, the capacity of the C-S-LNFP/Li cell demonstrates remarkably stable retention. Compared to the other two cells, the C-S-LNFP/Li cell delivers superior specific discharge capacities across

This article is licensed under a Creative Commons Attribution-NonCommercial 3.0 Unported Licence

Open Access Article. Published on 08 Oktober 2025. Downloaded on 16.10.25 03:04:51

**Journal Name** 

**ARTICLE** 

various current density conditions (Fig. S16). This performance strongly evidences that the Na<sup>+</sup> doping can enhance the rate ability of the cathode in the LFP. Furthermore, the C-S-LNFP/Li cell exhibits distinctly visible charge/discharge curves at different current densities, highlighting the notable advantages of the LNFP in the LSB. [43-45] Compared to similar works, this project demonstrates remarkable competitiveness (Table S3), convincingly showcasing the immense potential and value of the LNFP as a high-performance sulfur cathode additive for commercial use.

The key challenge for the commercialization of LSBs lies in achieving good cycling stability under high sulfur loading and at high current density conditions. Therefore, it is indispensable to conduct cycling performance tests on LSBs under such harsh conditions. At 5 C, the initial discharge specific capacities of C-S/Li, C-S-LFP/Li, and C-S-LNFP/Li cells are 384, 470, and 604 mAh g<sup>-1</sup>, respectively (Fig. 4b). Particularly noteworthy is that even under such demanding current density, the C-S-LNFP/Li cell can maintain a high discharge specific capacity, an achievement largely attributed to the excellent ion conductivity of the LNFP itself. As expected, the C-S-LNFP/Li cell still retains a discharge specific capacity of 548 mAh g<sup>-1</sup> after 300 cycles at 5 C, and this remarkable cycling stability performance is likely due to the inherent high stability of the LNFP. These results strongly demonstrate the superiority of Na<sup>+</sup> doping.

High sulfur loading cathodes were prepared, with the additive content maintained consistent with that in conventional sulfur loading cathodes. Subsequently, the assembled cells underwent cycling performance evaluations (Fig. S17). Unlike the cathode without any additives, which exhibits low discharge specific capacities (only 320 mAh g-1), the cathode with added the LNFP demonstrates higher discharge specific capacities (~880 mAh g-1) under high sulfur loading conditions (4.5 mg cm<sup>-2</sup>). This finding robustly confirms that even under harsh high sulfur loading conditions, the LNFP can also promote the redox reaction kinetics within the battery, thereby highlighting its vast application prospects and tremendous potential as a commercial sulfur cathode additive. A lithium-sulfur pouch cell incorporating the LNFP additive in the cathode was fabricated to evaluate its electrochemical performance. [46-48] It shows stable open circuit voltage of 2.96 V (Fig. S18a) and can power the light emittingdiode lamps (Fig. S18b) showing the capital letters of blurred 'SEU'.

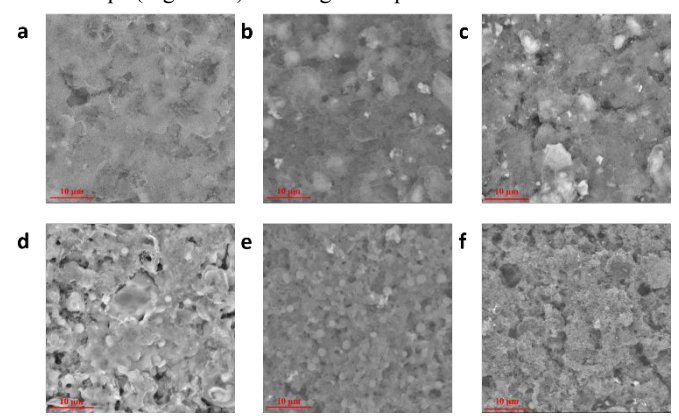


Fig. 5. SEM of cathodes: (a) C-S, (b) C-S-LFP, and (c) C-S-LNFP before cycling and (d~f) the corresponding ones after-cycling cathodes (1 C, 100 cycles).

After 100 cycles at 1 C, the cells were disassembled in an argonfilled glove box, and the cathodes were subjected to SEM testing. For direct comparison, the cathodes before cycling were also tested using SEM. The observation results indicated that the cathodes before cycling all exhibit a loose and porous structure (Figs. 152-26). 5176-44-464, the dense layers composed of deposited sulfur substances with lower electrochemical activity formed notably on the surfaces of the C-S (Fig. 5d) and C-S-LFP (Fig. 5e) post-cycled cathodes. The presence of these dense layers hinders the full utilization of active sulfur substances. In contrast, the post-cycled C-S-LNFP cathode retains a loose and porous structure (Fig. 5f) owing to the rapid ion transport channels enabled by the LNFP, a feature that promotes deep polysulfide penetration and diffusion. [49] This result intuitively highlights the advantages of the LNFP in the applications of LSBs.

With the aid of schematic illustrations, this paper visually demonstrates the notable advantages of the LNFP in LSB applications. In the absence of any functional cathode additives (Fig. 6a), the prepared LSBs generate soluble polysulfides during operation, which can easily penetrate the separator, leading to irreversible loss of active materials and accelerated corrosion of the lithium anode. This phenomenon poses a serious threat to the service life and safety of LSBs, greatly hindering their commercialization process. In contrast, when the LNFP is used as a functional additive for the cathode, its exceptional adsorption ability for sulfur substances anchors the generated polysulfides, preventing their unrestricted diffusion (Fig. 6b). Simultaneously, the LNFP can accelerate the catalytic conversion of soluble polysulfides into insoluble sulfides, ensuring efficient utilization of active sulfur substances. The enhanced ionic conductivity of the LNFP additionally ensures efficient ion transport, facilitating polysulfide diffusion within the cathode. The multifunctional effects of the LNFP contribute to a highperformance sulfur cathode.

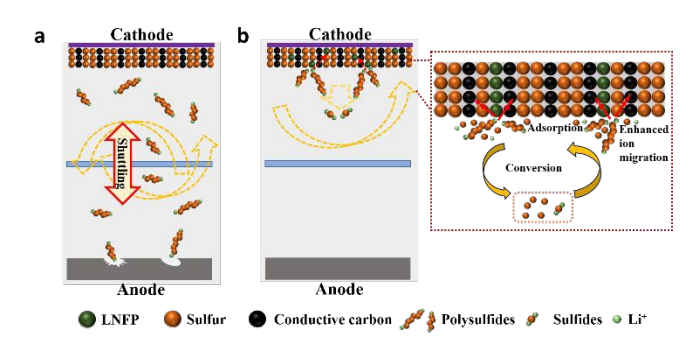


Fig. 6. Schematic diagrams of actions of the (a) C-S and (b) C-S-LNFP cathodes in LSBs (Insert: partial enlargement).

#### Conclusions

In summary, the micrometer-sized LNFP was successfully synthesized. We find that the prepared LNFP can effectively adsorb polysulfides due to the wide ion channels caused by Na<sup>+</sup> doping. Additionally, the Na<sup>+</sup> doping alters the electronic environment of Fe<sup>2+</sup>/Fe<sup>3+</sup>, which improves the intrinsic electronic conductivity of the LFP. The Na<sup>+</sup> doping also accelerates Li<sup>+</sup> diffusion, leading to improved ionic transport kinetics. Through theoretical calculations and experimental verification, the practical feasibility of the LNFP as a functional additive for the cathode of LSBs is confirmed. The LSB using the LNFP as an additive exhibits a capacity decay rate of only 0.039% per cycle after 700 cycles at 1 C. Even at high current density

ES Batteries Accepted Manuscrip

ARTICLE Journal Name

conditions of 5 C, the assembled LSB can stably cycle 300 times while maintaining a discharge specific capacity of approximately 600 mAh g<sup>-1</sup>. After cycling, no accumulation of non-conductive sulfur substances is observed on the surface of the cathode. This groundbreaking research addresses the current limitation of lithium salts as cathode additives with limited ionic conductivity and simultaneously broadens the selection scope of functional additive materials for cathodes, holding profound implications for the future commercialization of advanced LSBs.

#### **Experimental Section**

#### Preparation of the LFP and LNFP

The preparation of the LNFP is similar to previous reports. [33] Briefly, the Na<sub>2</sub>CO<sub>3</sub>, NH<sub>4</sub>H<sub>2</sub>PO<sub>4</sub>, FeC<sub>2</sub>O<sub>4</sub>·2H<sub>2</sub>O, and Li<sub>2</sub>CO<sub>3</sub> are meticulously measured and placed into an agate bowl by their stoichiometric proportions. The ensuing mixture undergoes ball milling at a speed of 400 rpm for 10 hours. Subsequently, the mixture is subjected to a thermal treatment process under the protective atmosphere of argon. The heated product is subjected to ball milling once again to obtain the desired LNFP powders. The LFP is prepared using the same method for comparison, except that the Na<sub>2</sub>CO<sub>3</sub> is not added.

#### Preparation of conventional sulfur loading cathodes

Firstly, acidified carbon nanotubes (CNTs) and sublimed sulfur are mixed uniformly at a mass ratio of 3:7. Subsequently, this mixture is placed into a Teflon liner filled with argon gas. Then, the liner is placed inside a reaction kettle, which is then positioned within a muffle furnace (155 °C, 12 h). After the temperature in the muffle furnace naturally drops to room temperature, the reaction kettle is removed. Finally, the retrieved sample is ground, yielding a carbon-sulfur (C-S) composite material.

The C-S composite, PVDF (polyvinylidene difluoride), and conductive carbon, with a mass ratio of 8:1:1, are placed into a small beaker. An appropriate amount of NMP (*N*-methyl pyrrolidone) is then added, and the mixture is magnetically stirred until a homogeneous slurry is formed. Subsequently, this slurry is poured onto the surface of an aluminum foil and spread evenly. After undergoing vacuum drying overnight, the aluminum foil coated with the slurry is cut into small circular discs with a diameter of 10 mm, thus successfully obtaining the C-S cathodes. The preparation process for the C-S-LFP and C-S-LNFP cathodes is similar to that of the C-S cathode. In both cases, the content of the LFP (LiFePO<sub>4</sub>) and LNFP in the cathode materials is controlled at 5 wt%. The sulfur loading is approximately 1.0 mg cm<sup>-2</sup>.

#### Preparation of high sulfur loading cathodes

High sulfur loading cathodes (4.5 mg cm<sup>-2</sup>) are prepared according to the previous report.<sup>[6]</sup> The carbon-sulfur composite, CMC (carboxymethyl cellulose), and conductive carbon (the mass ratio is 7:1:1) are added to deionized water containing dissolved CMC. The mixture is stirred until forming a homogeneous slurry. This slurry is coated onto carbon-coated aluminum foil. Then, the aluminum foil loaded with different materials is vacuum-dried overnight and cut into small circular discs to obtain high-loading cathodes. The preparation of C-S-LFP and C-S-LNFP high sulfur loading cathodes follows the same procedure as that for the C-S cathode, except that the LFP and LNFP are added to the slurry,

respectively. The content of functional additives in the high sulfur loading cathodes is controlled to be the same 1939/that 1941/1940 conventional sulfur loading cathodes.

#### Assembly of coin-type cells

A sulfur cathode, a separator, and a lithium metal anode are sequentially encapsulated inside a CR2025 coin shell in an argon-filled glove box ( $O_2$ <0.1 ppm,  $H_2O$ <0.1 ppm). After being compacted under a certain pressure, a lithium-sulfur cell is obtained. The electrolyte (LS-009) is dripped onto both sides of the separator, with the electrolyte quantity precisely controlled for each cell (40  $\mu$ L). The prepared lithium-sulfur cells are labeled as C-S/Li, C-S-LFP/Li, and C-S-LNFP/Li cells, respectively, based on the different cathodes used.

As for testing the catalytic performance of the LNFP towards polysulfides. The assembly process for the  $\text{Li}_2\text{S}_6$  symmetric cell is similar to that of the lithium-sulfur cell, with both the cathode and anode being the LNFP electrodes. The  $\text{Li}_2\text{S}_6$  electrolyte is dripped onto both sides of the separator. In addition, a pure LS-009 symmetric cell is prepared for comparison.

#### **Author Contributions**

We strongly encourage authors to include author contributions and recommend using <u>CRediT</u> for standardised contribution descriptions. Please refer to our general <u>author guidelines</u> for more information about authorship.

#### Conflicts of interest

There are no conflicts of interest to declare.

#### **Acknowledgements**

This work was supported by the Project on the National Natural Science Foundation of China (Key Project No. 52131306, and No. 22279016), Carbon Emission Peak and Neutrality of Jiangsu Province (No. BE2022031-4), the National Key Research and Development Program of China (No. 2021YFB2400400), the Fundamental Research Funds for the Central Universities (Nos. 2242023R10001, and 2242024K30047), the Start-up Research Fund of Southeast University (RF1028623005), the Zhishan Young Scholar Program of Southeast University (2242024RCB0004), SEU Innovation Capability Enhancement Plan for Doctoral Students (CXJH\_SEU 25075) and the Big Data Computing Center of Southeast University, the Postdoctoral Fellowship Program of CPSF under Grant Number GZC20250109, the China Postdoctoral Science Foundation under Grant Number 2025M770155.

#### References

- Z. Fan, Y. Li, J. Pan, Z. Zhou, W. Li, T. Yang, H. Zhang, C. Shu,
  W. Hua, Y. Wu, W. Tang, EES Batteries, 2025, 1, 100-118.
- **2** C. Wu, Z. Wang, Z. Jia, J. Cui, C. Shu, X. Wang, Y. Wu, W. Tang, *EES Batteries*, 2025, **1**, 364-384.
- 3 H. Liu, X. Liu, W. Li, X. Guo, Y. Wang, G. Wang, D. Zhao, Advanced Energy Materials, 2017, 7, 1700283.
- J. Guo, J. Huo, Y. Liu, W. Wu, Y. Wang, M. Wu, H. Liu, G. Wang, Small Methods, 2019, 3, 1900159.

**ARTICLE** Journal Name

29

- 5 S. Zheng, H. Geng, S. N. Eliseeva, B. Wang, Energy Materials, 2022, 2, 200042.
- 6 S. Xia, Z. Lin, B. Peng, X. Yuan, J. Du, X. Yuan, L. L. Liu, L. J. Fu, R. Holze, Y. P. Wu, Energy & Environmental Science, 2024, **17**, 5461.
- 7 T. Wang, J. He, X.-B. Cheng, J. Zhu, B. Lu, Y. Wu, ACS Energy Letters, 2022, 8, 116-150.
- S. Xia, X. Xu, W. Wu, Y. Chen, L. Liu, G. Wang, L. Fu, Q. 8 Zhang, T. Wang, J. He, Y. P. Wu, Materials Science and Engineering: R: Reports, 2025, 163, 100924.
- J. Song, S. Xia, N. Wang, J. Peng, B. Peng, W. Wu, L. Liu, X. Yuan, L. Fu, Y. Chen, Y. P. Wu, Advanced Materials, 2024, **37**, 2418295.
- 10 H. Song, K. Münch, X. Liu, K. Shen, R. Zhang, T. Weintraut, Y. Yusim, D. Jiang, X. Hong, J. Meng, Y. Liu, M. He, Y. Li, P. Henkel, T. Brezesinski, J. Janek, Q. Pang, Nature, 2025, 637, 846-853.
- 11 X. Pang, H. Geng, S. Dong, B. An, S. Zheng, B. Wang, Small, 2022, 19, 2205525.
- 12 J. Li, Z. Wang, K. Shi, Y. Wu, W. Huang, Y. Min, Q. Liu, Z. Liang, Advanced Energy Materials, 2023, 14, 2303546.
- 13 Q. Chen, J. Li, J. Pan, T. Li, K. Wang, X. Li, K. Shi, Y. Min, Q. Liu, Small, 2024, 20, 2401153.
- 14 K. Li, T. Li, Z. Wang, K. Shi, Y. Sun, J. Li, J. Ren, A. Lu, X. Li, Q. Liu, Advanced Functional Materials, 2024, 34, 2410517.
- 15 Z. Wang, W. Huang, H. Wu, Y. Wu, K. Shi, J. Li, W. Zhang, Q. Liu, Advanced Functional Materials, 2024, 34, 2409303.
- 16 T. Li, K. Shi, X. Li, W. Huang, J. Li, J. Li, K. Wang, Y. Deng, H. Chen, Y. Min, J. Li, Q. Liu, Advanced Functional Materials, 2025, 2505615,
- 17 X. Cui, X. Wang, Q. Pan, Energy Materials, 2023, 3, 300034.
- 18 S. Shen, L. Huang, X. Tong, R. Zhou, Y. Zhong, Q. Xiong, L. Zhang, X. Wang, X. Xia, J. Tu, Advanced Materials, 2021, 33, 2102796.
- P. Han, S. H. Chung, A. Manthiram, Small, 2019, 15, 19 1900690.
- 20 Z. Luo, W. Lei, X. Wang, J. Pan, Y. Pan, S. Xia, Journal of Alloys and Compounds, 2020, 812, 152132.
- 21 Z. Luo, X. Wang, W. Lei, P. Xia, Y. Pan, Journal of Materials Science & Technology, 2020, 55, 159-166.
- 22 P. Zhu, J. Zhu, C. Yan, M. Dirican, J. Zang, H. Jia, Y. Li, Y. Kiyak, H. Tan, X. Zhang, Advanced Materials Interfaces, 2018. **5**. 1701598.
- H. M. Kim, J.-Y. Hwang, S. Bang, H. Kim, M. H. Alfaruqi, J. 23 Kim, C. S. Yoon, Y.-K. Sun, ACS Energy Letters, 2020, 5, 3168-3175.
- H.-E. Wang, K. Yin, N. Qin, X. Zhao, F.-J. Xia, Z.-Y. Hu, G. Guo, 24 G. Cao, W. Zhang, Journal of Materials Chemistry A, 2019, 7, 10346-10353.
- 25 H. Lee, H. Nam, J. H. Moon, Energy Storage Materials, 2024, **70**, 103551.
- 26 N. Li, T. Meng, L. Ma, H. Zhang, J. Yao, M. Xu, C. M. Li, J. Jiang, Nano-Micro Letters, 2020, 12, 145.
- 27 K. Sun, M. Fu, Z. Xie, D. Su, H. Zhong, J. Bai, E. Dooryhee, H. Gan, Electrochimica Acta, 2018, 292, 779-788.
- 28 M. Zheng, X. Gao, Y. Sun, K. Adair, M. Li, J. Liang, X. Li, J. Liang, S. Deng, X. Yang, Q. Sun, Y. Hu, Q. Xiao, R. Li, X. Sun, Small Methods, 2021, 5, 2100176.

- S. Xia, J. Song, Q. Zhou, L. L. Liu, J. L. Ye, T. Wang, Y. H. Chen, Y. K. Liu, Y. P. Wu, T. Ree, Advanced 15cierae, 52023,140, 2301386.
- 30 S. Xia, Z. Chen, L. Yuan, J. Song, Q. Zhou, X. Yuan, L. Liu, L. Fu, Y. Chen, Y. Wu, Journal of Materials Chemistry A, 2023, 11, 19870-19876.
- X. Gao, C. Zheng, Y. Shao, V. R. Shah, S. Jin, J. Suntivich, Y. 31 L. Joo, ACS Applied Materials & Interfaces, 2023, 15, 19011-19020.
- 32 S.-P. Chen, D. Lv, J. Chen, Y.-H. Zhang, F.-N. Shi, Energy & Fuels, 2022, 36, 1232-1251.
- B. Peng, Z. Liu, Q. Zhou, X. Xiong, S. Xia, X. Yuan, F. Wang, K. I. Ozoemena, L. Liu, L. Fu, Y. P. Wu, Advanced Materials, 2023, 36, 2307142.
- 34 E. M. Lotfabad, J. Ding, K. Cui, A. Kohandehghan, W. P. Kalisvaart, M. Hazelton, D. Mitlin, ACS Nano, 2014, 8, 7115-7129.
- 35 C. Barchasz, F. Molton, C. Duboc, J. C. Lepretre, S. Patoux, F. Alloin, Analytical Chemistry, 2012, 84, 3973-3980.
- Q. Liang, S. Wang, X. Lu, X. Jia, J. Yang, F. Liang, Q. Xie, C. 36 Yang, J. Qian, H. Song, R. Chen, ACS Nano, 2024, 18, 2395-
- 37 C. Shang, L. Cao, M. Yang, Z. Wang, M. Li, G. Zhou, X. Wang, Z. Lu, Energy Storage Materials, 2019, 18, 375-381.
- 38 J. Xu, S. An, X. Song, Y. Cao, N. Wang, X. Qiu, Y. Zhang, J. Chen, X. Duan, J. Huang, W. Li, Y. Wang, Advanced Materials, 2021, 33, 2105178.
- X. Liang, C. Hart, Q. Pang, A. Garsuch, T. Weiss, L. F. Nazar, 39 Nat. Commun., 2015, 6, 5682.
- 40 E. Jing, L. Chen, S. Xu, W. Tian, D. Zhang, N. Wang, Z. Bai, X. Zhou, S. Liu, D. Duan, X. Qiu, Journal of Energy Chemistry, 2022, 64, 574-582.
- D. Yang, L. He, Y. Liu, W. Yan, S. Liang, Y. Zhu, L. Fu, Y. Chen, 41 Y. Wu, Journal of Materials Chemistry A, 2019, 7, 13679-
- A. Zhang, X. Fang, C. Shen, Y. Liu, I. G. Seo, Y. Ma, L. Chen, 42 P. Cottingham, C. Zhou, Nano Research, 2018, 11, 3340-
- 43 J. Zhou, C. Shu, J. Cui, C. Peng, Y. Liu, W. Hua, L. Simonelli, Y. Wu, S. X. Dou, W. Tang, *Carbon Energy*, 2024, **6**, e460.
- 44 Y. Ding, T. Yan, J. Wu, M. Tian, M. Lu, C. Xu, J. Gu, H. Zhao, Y. Wang, X. Pan, S. X. Dou, L. Zhang, J. Sun, Applied Catalysis B: Environmental, 2024, 343, 123553.
- Q. Lv, Y. Sun, B. Li, C. Li, Q. Zhang, L. Wang, Advanced 45 Energy Materials, 2025, 15, 2403223.
- 46 Y. Song, X. Long, Z. Luo, C. Guo, C.-N. Geng, Q.-S. Ouyang, Z. Han, G. Zhou, J.-J. Shao, ACS Applied Materials & Interfaces, 2022, 14, 32183-32195.
- 47 Y. Song, H. Li, J. Li, J. An, J.-J. Shao, G. Zhou, Journal of Energy Chemistry, 2023, 87, 51-60.
- 48 Y. Song, M. Zhou, Z. Chen, H. Nie, J.-J. Shao, G. Zhou, Chinese Chemical Letters, 2024, **35**, 109200.
- 49 H. Yao, K. Yan, W. Li, G. Zheng, D. Kong, Z. W. Seh, V. K. Narasimhan, Z. Liang, Y. Cui, Energy & Environmental Science, 2014, 7, 3381-3390.

S Batteries Accepted Manus

**EES Batteries Accepted Manuscript** 

View Article Online DOI: 10.1039/D5EB00160A

## **Data Availability**

The data supporting this article have been included as part of the ESI.†